Front. Environ. Sci. Eng. 2022, 16(10): 130
https://doi.org/10.1007/s11783-022-1565-0

RESEARCH ARTICLE

Tailoring the simultaneous abatement of methanol and NO_x on Sb-Ce-Zr catalysts via copper modification

Xiaoqiang Wang[1,2], Yanye Zhu[1], Yue Liu (✉)[1], Xiaole Weng[1], Zhongbiao Wu[1]

1 Department of Environmental Engineering, Zhejiang University, Hangzhou 310058, China
2 College of Biological, Chemical Science and Engineering, Jiaxing University, Jiaxing 314001, China

HIGHLIGHTS

- Cu addition enhances CH_3OH oxidation and alleviates its inhibitory effect on SCR.
- Cu addition improves the activation of SCR reactants in the presence of methanol.
- Damaged structure by more Cu addition decreases specific surface area and acidity.
- Excessive Cu addition would lead to the narrowing of SCR temperature window.

GRAPHIC ABSTRACT

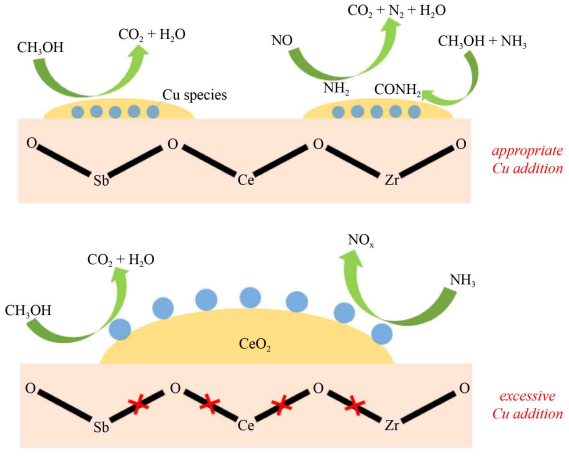

ARTICLE INFO

Article history:
Received 30 December 2021
Revised 30 January 2022
Accepted 16 February 2022
Available online 28 March 2022

Keywords:
Copper modification
Sb-$CeZr_2O_x$ catalyst
NO_x
Methanol
Simultaneous removal

ABSTRACT

Simultaneously removal of NO_x and VOCs over NH_3-SCR catalysts have attracted lots of attention recently. However, the presence of VOCs would have negative effect on deNO_x efficiency especially at low temperature. In this study, copper modification onto $Sb_{0.5}CeZr_2O_x$ (SCZ) catalyst were performed to enhance the catalytic performance for simultaneous control of NO_x and methanol. It was obtained that copper addition could improve the low-temperature activity of both NO_x conversion and methanol oxidation, where the optimal catalyst ($Cu_{0.05}$SCZ) exhibited a deNO_x activity of 96% and a mineralization rate of 97% at 250 °C, which are around 10% higher than that of Cu free sample. The characterization results showed that copper addition could obviously enhance the redox capacity of the catalysts. As such, the inhibition effect of methanol incomplete oxidation on NO adsorption and NH_3 activation were then lessened and the conversion of surface formamide species were also accelerated, resulting in the rising of NO_x conversion at low temperature. However, excessive copper addition would damage the Sb-Ce-Zr oxides solid solution structure owing to Cu-Ce strong interactions, decreasing the surface area and acidity. Meanwhile, due to easier over-oxidation of NH_3 with more Cu addition, the temperature window for NO_x conversion would become quite narrow. These findings could provide useful guidelines for the synergistic removal of VOCs over SCR catalyst in real application.

1 Introduction

Nitrogen oxides (NO_x) and volatile organic compounds (VOCs) are two main kinds of air pollutants in current China (Kang et al., 2019; Qu et al., 2020; Sun et al., 2021), which would cause the secondary pollution of ozone and $PM_{2.5}$ (Chu et al., 2020; Wang et al., 2020a). Recently, owing to the improved utilization of energy and spacing (Gan et al., 2021; Huang et al., 2021), the simul-

✉ Corresponding author
E-mail: yueliu@zju.edu.cn

taneous removal of NO_x and VOCs in single catalytic reactor, combining NH_3-SCR technology and VOCs catalytic oxidation, have drawn widespread attention (Long et al., 2021; Zhai et al., 2021). Typical VOCs, such as chlorobenzene (Gan et al., 2018) and toluene (Ye et al., 2020), were involved in current studies, where the most common SCR catalysts applied to explore the simultaneous removal of NO_x and VOCs were V-Ti based catalysts (Wang et al., 2021a; Ye et al., 2020). Although highly reactivity in dehydrochlorination of chlorinated alkanes and good resistance to the toxicity of chlorine could be achieved, poor removal efficiency for hydrocarbons and oxygenated compounds, owing to the insufficient oxidative capacity (Li et al., 2012; Liang et al., 2017), still hindered their practical application for medium/low temperature NH_3-SCR and VOCs catalytic combustion (Li et al., 2012; Liang et al., 2017; Wang et al., 2021a). Therefore, it is significant interest in developing high activity catalysts with wide temperature window for simultaneous removal of NO_x and VOCs.

As one of the important chemical compounds, nitromethane has been applied in many industries (Ambekar et al., 2018), while its production process often generates high concentration of NO_x and certain amount of methanol. And it is essential to address the pollution caused by the nitromethane production process in an energy-efficient and convenient way. As a promising candidate NH_3-SCR catalyst for real applications, ceria based catalysts had been widely researched owing to the shifting valence state of cerium and the oxygen defects (Li et al., 2017; Zhang et al., 2022). Recently, Sbpromoted $CeZr_2O_x$ NH_3-SCR catalysts have been reported as their superior low/medium temperature activity owing to the well redox capacity and surface acidity (Wang et al., 2020d, 2021b). And the optimized $Sb_{0.5}CeZr_2O_x$ catalyst had been applied for the simultaneous removal of NO_x and methanol in our previous study (Zhu et al., 2021), which had achieved good synergistic performance for NO_x and methanol removal in the medium temperature range. However, the co-existence of methanol exhibited an obviously negative impact on the deNO_x activity below 250 °C, especially when the concentration of methanol was higher than that of NO, which was ascribed to the unsatisfied mineralization rate of methanol. In other words, the working temperature window of the catalyst should be broadened in further works and try to fit the real tail gas temperature range, where one important point was to improve the simultaneous removal efficiency of NO_x and methanol at low temperature.

To enhance the mineralization rate of methanol in the medium-low temperature, the redox capacity of the Sb-Ce-Zr catalyst should be promoted. According to previous literatures (Wang et al., 2020b; Wang et al., 2020c), due to the advantages of cheap, non-toxic and low temperature reducibility, the transition metal Cu has been widely applied in the VOCs catalytic oxidation and low-temperature NH_3-SCR. What's more, the synergistic effect between Cu and Ce could promote the redox ability and then be favor to the low temperature activity (Ali et al., 2017; Zeng et al., 2021). Thus, the modification of copper could be practical and feasible to tailor the simultaneous abatement of methanol and NO_x on Sb-Ce-Zr catalyst. Therefore, in this paper, the $Sb_{0.5}CeZr_2O_x$ catalyst was modified by addition different content of Cu during the citrate method synthesized process. The influence of Cu modification on the catalytic performance was then investigated, where the physicochemical properties and reactants adsorption reaction characteristics of the catalysts after copper modification were characterized to determine their performances in simultaneous abatement of methanol and NO_x.

2 Experimental section

2.1 Catalysts preparation

The $Sb_{0.5}CeZr_2O_x$ catalyst was synthesized by the citrate method reported in our previous works (Wang et al., 2019; Wang et al., 2020d; Zhu et al., 2021). The Cu-modified $Sb_{0.5}CeZr_2O_x$ catalysts were prepared in a similar way as follows. A different amount of copper nitrate ($Cu(NO_3)_2{\cdot}3H_2O$) was added to the solution of antimony acetate ($C_6H_9O_6Sb$), cerium nitrate ($Ce(NO_3)_3{\cdot}6H_2O$), and zirconium nitrate ($ZrO(NO_3)_2{\cdot}xH_2O$), and then mixed with the citric acid ($C_6H_8O_7$) whose molar amount is 1.5 times that of the total metal cations. The prepared catalyst is labeled as Cu_xSCZ, where "x" represents the atomic ratio of Cu to Ce, and "SCZ" stands for $Sb_{0.5}CeZr_2O_x$.

2.2 Catalysts characterization

N_2 adsorption-desorption isotherms were measured using a Beijing JWGB adsorption apparatus. Before the measurement, the catalysts were degassed at 200 °C for 90 min. Surface areas were determined by the Brunauer-Emmett-Teller (BET) method. Pore volumes and average pore sizes were determined from the desorption branch of isotherms by the Barret-Joyner-Halenda (BJH) method. X-ray diffraction with Cu Kα radiation (XRD: model Bruker D8 Advance instrument, Germany) was applied to analyze the crystal phases of all the samples with scattering angles (2θ) ranging between 10° and 80° at a scanning velocity of 5°/min. Raman spectra were obtained from a Renishaw in Via Raman spectrometer using a light source at 532 nm. Transmission electron microscopy (TEM) and high-resolution (HR) TEM images were taken from a Tecnai G2 F20 S-TWIN transmission electron microscope. X-ray photoelectron spectroscopy (XPS) was performed on a Thermo Scientific K-Alpha spectrometer equipped with a standard Al Kα source with a calibration of C1s peak at 284.8 eV. Temperature-programmed desorption

(TPD), temperature-programmed reduction (TPR), and temperature-programmed oxidation (TPO) experiments were performed using a TP5079 analyzer equipped with a HIDEN QGA mass spectrometer and a thermal conductivity detector. In the temperature-programmed desorption (TPD), temperature-programmed reduction (TPR), and temperature-programmed oxidation (TPO) experiments, 100 mg catalyst in 40–60 mesh was pretreated in He stream at 400 °C for 1 h each time, and then cooled down to the required temperature. The cylinder gases of NH_3, NO, CH_3OH, and O_2 were balanced by He, while the H_2 was mixed with N_2. The programed heating rate was set as 10 °C/min. The concentrations of mixed gases used in different tests were listed in Table S1. In situ Diffuse Reflectance Infrared Transform Spectroscopy (DRIFT) was measured using a Bruker Tensor 27 Infrared spectrometer from 4000 to 1000 cm^{-1} with a scanning frequency of 32 times each minute. Before each experiment, the catalyst below 100 mesh was pretreated at 400 °C for 1 h in He stream, and then cooled down to 200 °C for the collection of background spectrum. In the typical NH_3 adsorption experiment, the catalyst was exposed to 0.10% NH_3 for 30 min. To obtain DRIFT spectra of NO adsorption on two catalysts pretreated with methanol, the catalysts were first exposed to 0.06% CH_3OH and then purged with He until the signals stabilized, followed by the exposure to 0.06% NO + 5% O_2. The time-dependent spectra were collected by subtracting the stable spectra after He purging. In the transient study of Eley-Rideal (E-R) reaction pathway, the "untreated" sample was exposed to 0.06% NH_3 for 30 min and then turned to 0.06% NO + 5% O_2. The "pretreated" sample was pre-adsorbed with 0.06% CH_3OH and then purged with He to collect the background spectrum. Afterwards, the experimental steps were as same as those of "untreated" sample.

2.3 Catalytic performance evaluation tests

Catalytic activity tests and stability tests were conducted using a fixed-bed reactor system. All catalysts were sieved to 40−60 mesh before tests. The typical flow was composed of 0.06% NO, 0.06% NH_3, 0.12% CH_3OH, 5 vol.% O_2, 5 vol.% H_2O, and balanced N_2, adding up to 1.5 L/min corresponding to a gas hourly space velocity (GHSV) of 100 000 h^{-1}. Methanol and water were introduced into the feed system via gas blowing while other components came from cylinder gases.

The NO, NO_2, and O_2 concentrations were monitored using an infrared flue gas analyzer (MRU MGA5, Germany). CH_3OH and CO_x were measured using a gas chromatograph (GC7890A, Agilent Technologies, USA). N_2O was detected by a small analyzer (G200, Bedfont Inc., UK). NH_3 concentration was quantified using an ultraviolet flue gas analyzer (3020A, SHIYI Co., China). The main performance indicators were calculated by following equations:

$$NO_x \text{ conversion} = \left(1 - \frac{NO_{out} + NO_{2out}}{NO_{in} + NO_{2in}}\right) \times 100\% \quad (1)$$

$$N_2 \text{ selectivity} = \left(1 - \frac{N_2O_{out}}{NO_{in} + NO_{2in} - NO_{out} - NO_{2out}}\right) \times 100\% \quad (2)$$

$$CH_3OH \text{ conversion} = \left(1 - \frac{CH_3OH_{out}}{CH_3OH_{in}}\right) \times 100\% \quad (3)$$

$$CO_2 \text{ yield} = \frac{CO_{2out}}{CH_3OH_{in}} \times 100\% \quad (4)$$

where "in" and "out" subscripts indicate the inlet and outlet concentrations, respectively.

3 Results and discussion

3.1 Simultaneous catalytic abatement performance

Simultaneous catalytic abatement performance of methanol and NO_x over Cu_xSCZ catalysts (x = 0, 0.02, 0.05, 0.1) have been evaluated by activity tests. As shown in Fig. 1a, the deNO_x efficiency at low temperatures in the presence of methanol increased with the addition of Cu. Taking the activity of NH_3-SCR in the absence of methanol (see Fig. S1) as a contrast, the addition of Cu could mitigate the inhibitory effects of methanol on the deNO_x activity, where the N_2 selectivity was influenced to a lesser extent (Fig. 1b). For instance, the deNO_x activity of $Cu_{0.05}SCZ$ sample at 200 °C increased by 6% compared to that of SCZ sample under the condition of CH_3OH/NO = 2. Such effect would be more evident at CH_3OH/NO = 1 as the NO_x conversion gap between these two samples enlarged to about 17% (see Fig. S2). However, excessive addition of Cu (see $Cu_{0.1}SCZ$ sample) obviously narrowed the working temperature window for SCR reaction, which might be ascribed to over-oxidation of ammonia at high temperatures range (Wang et al., 2020b). Meanwhile, it was found the methanol conversion rate and CO_2 yield for Cu_xSCZ samples greatly improved with Cu contents at low temperatures (< 250 °C) (see Figs. 1c and 1d). Specifically, the CO_2 yield of $Cu_{0.05}SCZ$ sample increased by around 20% than SCZ catalyst at 200 °C. It might be mainly ascribed to the enhanced oxidative capacity of catalysts after copper modification, as it could be obviously observed that the methanol conversion and mineralization rate were improved for CH_3OH solo oxidation (see Fig.S1). Considering overall removal efficiency of methanol and NO_x, $Cu_{0.05}SCZ$ sample should be the optimal catalyst,

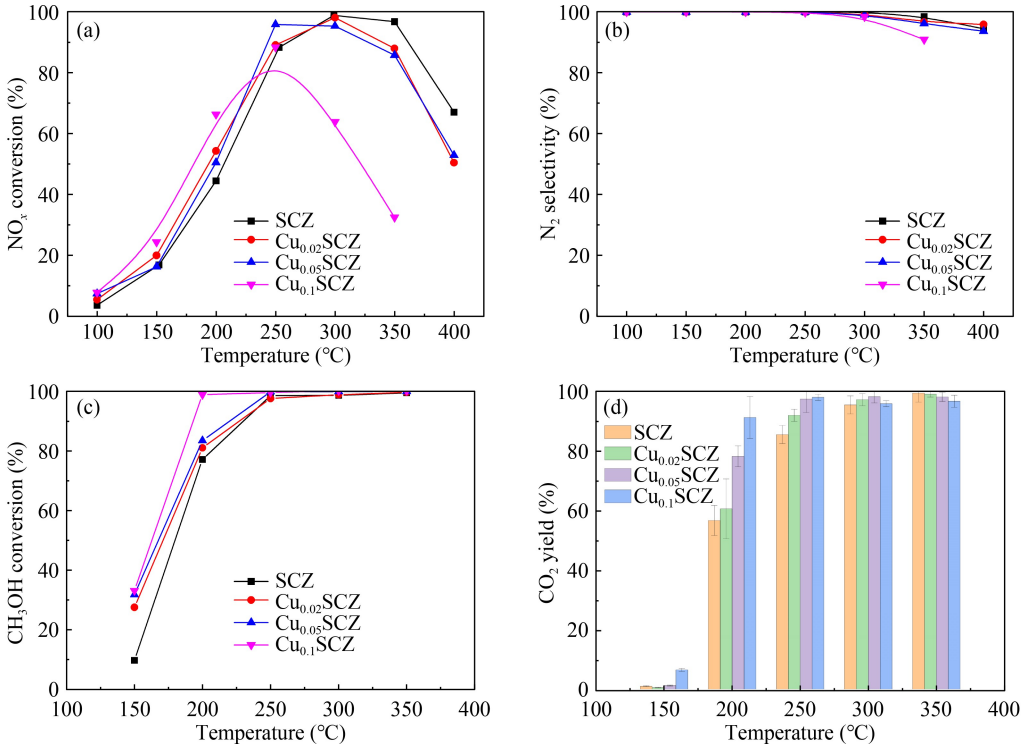

Fig. 1 The simultaneous catalytic abatement performance of methanol and NO_x over Cu_xSCZ catalysts: (a) deNO_x activity, (b) N_2 selectivity, (c) CH_3OH conversion, and (d) CO_2 yield. Reaction conditions: [NO] = [NH_3] = 0.06%, [CH_3OH] = 0.12%, [O_2] = 5 vol.%, [H_2O] = 5 vol.%, N_2 balance, GHSV = 100, 000 h^{-1}.

where over 85% deNO_x efficiency and more than 90% N_2 selectivity in the range of 250–350 °C could be achieved, and methanol conversion and CO_2 yield both exceed 95% at the same time. Furthermore, stability tests on $Cu_{0.05}SCZ$ catalyst at temperature 250 °C and 325 °C had also been carried out. As shown in Fig. S3, $Cu_{0.05}SCZ$ catalyst could maintain 90% or above in methanol conversions, CO_2 yields, NO_x conversion and N_2 selectivity at both temperatures during reaction running time of 12 h. Such fact confirmed that $Cu_{0.05}SCZ$ sample was able to work stably at temperature over than 250 °C.

3.2 Structural and chemical properties

The basic physical properties of catalysts, including specific surface area, pore volume and pore size, have been measured by nitrogen adsorption-desorption apparatus and analyzed by BET-BJH method. As shown in Table 1, specific surface area of SCZ catalyst was 94 m^2/g, and it was a considerable value due to the strong interaction between Sb and Ce-Zr oxides. Compared to the physical properties of pristine SCZ sample, the investigated catalysts with low copper contents ($Cu_{0.02}SCZ$ and $Cu_{0.05}SCZ$) possessed slightly larger specific surface area and pore volume. It could be speculated that addition of a small amount of Cu would generate more micro-pores possibly due to the interaction of Cu with other components. However, when Cu content increased to 10% of Ce, the specific surface area decreased obviously, which might be ascribed to the blockage of partial pores or the damaged structure of Sb-Ce-Zr oxides solid solution by excessive copper addition.

Typically, XRD and Raman Spectroscopy had been applied to analyze crystal structure of Cu_xSCZ catalysts. As shown in Fig. 2a, the obvious diffraction peaks located at 29.3°, 33.7°, 48.8°, and 58.1° could be subjected to the solid solution of cerium and zirconium oxide in PDF#38-1436. With the addition of copper, no significant shift of the diffraction peak position was observed in Cu_xSCZ catalysts, while the half-width was

Table 1 Physical information and calculated XPS results of Cu_xSCZ catalysts

Sample	Specific surface area(m^2/g)	Total pore volume(cm^3/g)	Average pore size(nm)	Ce^{3+}/Ce_{total}	O_β/O_{total}	Cu^+/Cu_{total}
SCZ	94	0.07	3.87	0.34	0.13	–
$Cu_{0.02}SCZ$	95	0.07	3.51	0.41	0.14	–
$Cu_{0.05}SCZ$	105	0.08	3.90	0.42	0.20	0.61
$Cu_{0.1}SCZ$	74	0.06	4.34	0.34	0.26	0.57

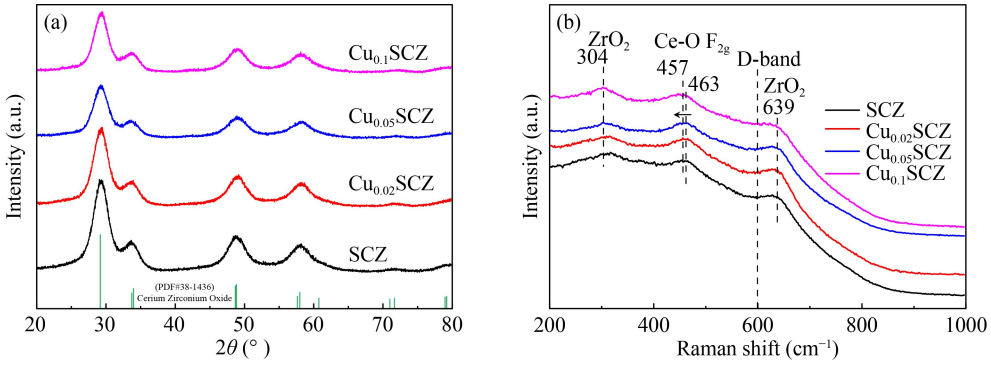

Fig. 2 XRD patterns (a) and Raman spectra (λ = 532 nm) (b) of the Cu_xSCZ samples.

increased. And it was indicated that the presence of Cu could induce the reduction of crystallinity and particle size in the mixed oxides, which was in accordance with BET-BJH results. Additionally, no characteristic peak of CuO was observed in all XRD patterns, suggesting a high dispersion of Cu in all Cu_xSCZ catalysts.

Furthermore, based on the previous works (Gao et al., 2013; Wang et al., 2019), the dominant peaks at 304 and 639 cm^{-1} in Fig. 2b could be attributed to the monoclinic structure of ZrO_2, while the typical peak located at 464 cm^{-1} was subjected to the F_{2g} symmetric vibration (O-Ce-O stretching) of the cubic fluorite structure. Importantly, the formation of Ce-Zr oxides solid solution would induce a blue shift of the F_{2g} peak (Taniguchi et al., 2010), while the further introduction of Sb into Ce-Zr oxides solid solution would bring about a red shift (Wang et al., 2019). And it was the reason that the F_{2g} peak in the spectrum of SCZ sample shifted to 463 cm^{-1} in Fig. 2b. Notably, after the additionally of Cu, the F_{2g} peak of ceria would gradually shift from 463 to 457 cm^{-1}, where the significantly shifted Raman characteristic peak of ceria could be due to the formation of strong interaction between copper and cerium (Ali et al., 2017). And the widened half-width of the F_{2g} peak also confirmed the reduced particle size and the increased specific surface area after copper modification in XRD and BET-BJH results, as half-width of peak is inversely proportional to the particle size (Graham et al., 1991), which further verified the formation of strong Cu-Ce interactions. In particular, the decreased specific surface area of $Cu_{0.1}$SCZ sample in Table 1 indicated that the excessive addition of Cu would damage the existed Sb-Ce-Zr oxides solid solution structure owing to Cu-Ce strong interactions, which were in consistent with the previous work (Ali et al., 2017). And the slightly increased XRD peak intensity of $Cu_{0.1}$SCZ sample compared to $Cu_{0.05}$SCZ sample could also be corroborative evidence.

To further observe the morphology and discover the fine structure information, the SCZ, $Cu_{0.05}$SCZ, and $Cu_{0.1}$SCZ samples were studied by TEM characterization. Seeing from Fig. 3, all irregular aggregates composed of nano particles could be observed in the investigated samples. In detail, the lattice fringes in SCZ catalyst indicated that the main crystalline structure was cerium

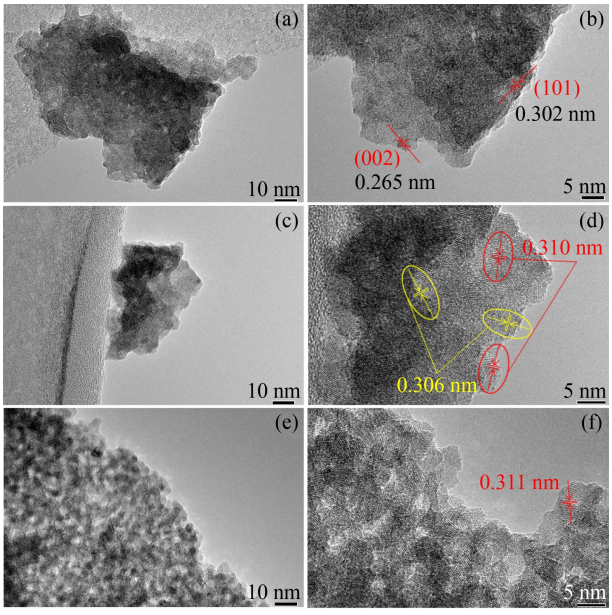

Fig. 3 HRTEM images for (a, b) SCZ, (c, d) $Cu_{0.05}$SCZ, and (e, f) $Cu_{0.1}$SCZ samples.

zirconium oxides solid solution, which was in line with the XRD pattern. Specially, the lattice stripes with spacing of 0.302 nm and 0.265 nm could be identified as the reference values in PDF#38-1436 (3.05 Å and 2.65 Å corresponding to (101) and (002) crystal planes, respectively). In zirconium-rich Ce-Zr oxides solid solution, due to the larger ionic radius of Ce^{4+} (0.97 Å) than Zr^{4+} (0.84 Å) (Reddy et al., 2007), the doping of Ce^{4+} into the ZrO_2 lattice would lead to a larger lattice spacing, but still smaller than CeO_2. After the introduction of a certain amount of Cu, some Cu^{2+} (0.73 Å) would form strong interactions with Ce, leading to cell deformation (Zeng et al., 2021). As a consequence, an expansion in lattice stripe for Ce-Zr oxides solid solution from 0.302 to 0.306 nm could be observed. As for the lattice fringes with a spacing of 0.310 and 0.311 nm founded in $Cu_{0.05}$SCZ and $Cu_{0.1}$SCZ sample, it could basically be considered as CeO_2 crystals. This might be due to the fact that high amount of Cu species could hinder the entry of Ce into the ZrO_2 lattice to some extent, forming CeO_2 crystal

structures in local micro-regions. Although no crystalline phase of CuO was found in the vicinity, some regions lacking regular lattice stripes were observed. And combined with the information of decreased crystallinity in XRD results, it could be deduced that the existence of Cu did change the metal-metal interactions in Sb-Ce-Zr oxides, inducing the larger lattice spacing during cell deformation by the interaction of Cu-Ce. And excessive Cu addition would result in the destruction of Sb-Ce-Zr oxides solid solution structure.

Moreover, the chemical states of different elements on the catalysts surface were analyzed by XPS measurement. The XPS spectra of Ce 3d, O 1s and Cu 2p3/2 for all catalysts were illustrated in Fig. 4 and the surface atomic contents of the elements were summarized in Table 1. Generally, Ce 3d spectra could be unfolded into ten peaks (Wang et al., 2018; Wang et al., 2019), where four peaks marked were subjected to Ce^{3+} and the remaining unmarked peaks were assigned to Ce^{4+}. O 1s peaks could be divided into three sub-peaks: lattice oxygen O_α (529.0–530.0 eV), chemisorbed oxygen O_β (531.3–531.9 eV) and hydroxyl oxygen O_γ (532.7–533.5 eV) (Hu et al., 2016). Moreover, in Cu 2p3/2 spectra, owing to the low Cu content, the distinguishable peaks could be hardly detected in $Cu_{0.02}$SCZ sample. As for other two samples, two broad peaks located at 934.1 and 932.2 eV emerged, suggesting the coexistence of Cu(II) and Cu(I) (Lu et al., 2019). As shown in Table 1, except the $Cu_{0.1}$SCZ sample, the ratio of Ce^{3+} and O_β were both increased after Cu addition. Based on the previous works (Wang et al., 2019; Yao et al., 2019), the ratio of Ce^{3+} and O_β were mutually corroborating to the redox ability. These results indicated that the addition of Cu truly promoted the reducibility of SCZ sample. However, focusing on the relationship among O_β, Ce^{3+} and Cu^+ in $Cu_{0.1}$SCZ sample, it could be found that the ratio of Ce^{3+} decreased but the proportion of O_β increased. The above contradictory results might further indicate that the excessive addition of Cu would damage the interaction between Sb-Ce-Zr by strong Cu-Ce interactions as suggested in TEM analysis. Additionally, the shift to higher binding energies in the XPS peaks of Sb and Zr after Cu addition (see Fig. S4) could also support it. For SCZ sample, the interactions between Sb-Ce-Zr would generate certain amount of Ce^{3+} and O_β. After low content Cu addition, the strong Cu-Ce interaction would be formed with little effect on Sb-Ce-Zr crystal structure and then both the ratio of Ce^{3+} and O_β increased. However, with the excessive addition of Cu, such strong interactions between Cu-Ce would disrupt the formal formed Sb-Ce-Zr interactions and more amount of Ce species exist in ceria phase, which finally decreased the Ce^{3+} content. Though the Ce^{3+} ratio decreased, more CuO_x species in the vicinity of ceria would be also beneficial to the increase of chemisorbed oxygen O_β.

3.3 Surface acidity and reducibility

The surface acidity of catalysts has been characterized by NH_3-TPD experiments, and the results are shown in Fig. 5. From Fig. 5a, two wide desorption peaks at 100–400 °C and 400–600 °C could be observed in all samples. The former could be attributed to the desorption peak of

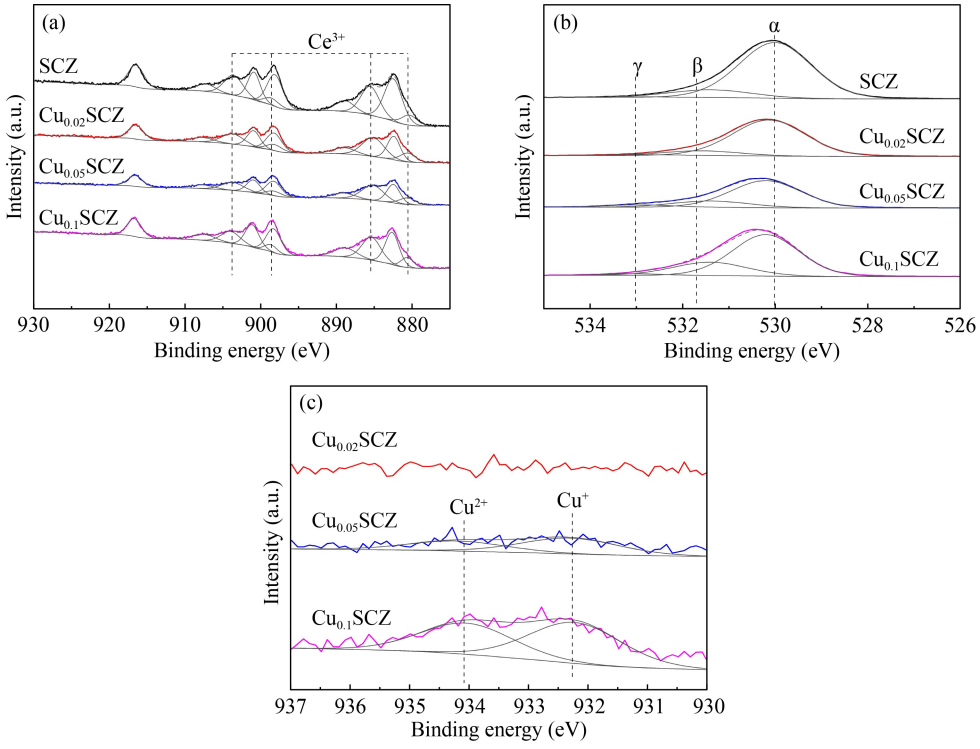

Fig. 4 XPS spectra of (a) Ce 3d, (b) O 1s, and (c) Cu 2p3/2 in the Cu_xSCZ samples.

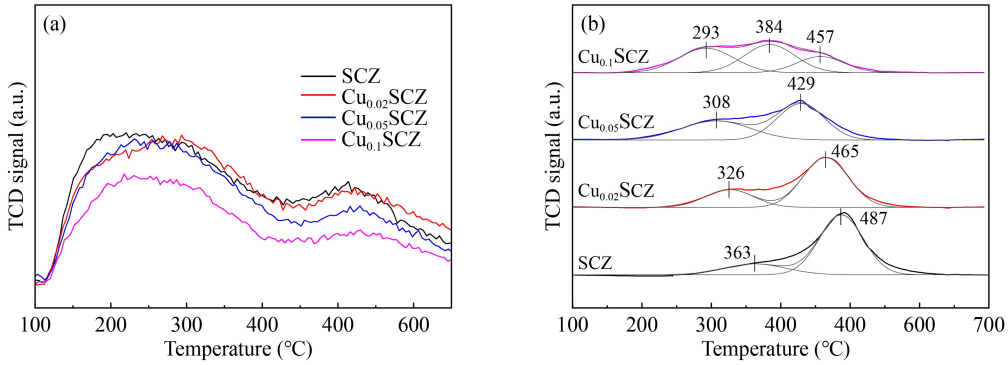

Fig. 5 NH_3-TPD (a) and H_2-TPR (b) profiles of the Cu_xSCZ catalysts.

physically adsorbed NH_3 and NH_4^+ adsorbed at Brønsted acid sites, while the latter was assigned to the desorption peak of coordinated NH_3 at Lewis acid sites (Zhou et al., 2020). With the increase of copper content, the loss of strong Lewis acid sites became more and more obvious compared with SCZ sample. As the acidity of SCZ sample was mainly derived from the Ce-O-Sb structure (Wang et al., 2019; Wang et al., 2020d), the decreased acidity after copper modification could further confirm that the addition of Cu would form the strong interactions with Ce and then gradually damage the existed Sb-Ce-Zr structures. And the significant weakened acidity in $Cu_{0.1}$SCZ could partly account for its decreased deNO_x efficiency at high temperature range due to the over-oxidation of ammonia. Furthermore, the NH_3-IR spectra in Fig. S5 was also in consistent with the NH_3-TPD results, where the addition of Cu did show negative effect on the surface acidity of the catalyst.

As the H_2-TPR profiles shown in Fig. 5b, it could be found that the emerged reduction peaks were within the temperature range of 200–600 °C. For pure SCZ catalyst, the emerged two reduction peaks could be both ascribed to surface CeO_2 species, corresponding to the reduction of oxygen species in Ce-O-Ce and Ce-O-Sb structure, respectively (Wang et al., 2019). After the addition of Cu, the reduction peaks were shifted to the low temperature region as a whole, which was unsurprisingly due to the promoting effect of Cu in reducibility. Particularly, for $Cu_{0.1}$SCZ sample, the first reduction peak was shifted to the lower temperature (below 300 °C), and the second peaks were divided into two sub-peaks. As the reduction peaks of CeO_2 could not be found below 300 °C and pure zirconia or antimony species cannot be reduced in hydrogen below 600 °C (Wang et al., 2019; Wang et al., 2020d), thus, the first reduction peak in $Cu_{0.1}$SCZ sample should be mainly ascribed to highly dispersed CuO_x interacted with ceria (Ali et al., 2017). In comparison, the first reduction peak in $Cu_{0.02}$SCZ and $Cu_{0.05}$SCZ samples should be subjected to the overlapped reduction peaks of CuO_x species and Ce-O-Ce structure. Moreover, ceria-based species should still be responsible for the emerged reduction peaks above 350 °C. Specifically, the reduction peaks (located at 465 °C in $Cu_{0.02}$SCZ, 429 °C in $Cu_{0.05}$SCZ and 457 °C in $Cu_{0.1}$SCZ) were due to the reduction of Ce-O-Sb structure. And the peak located at 384 °C in $Cu_{0.1}$SCZ sample was assigned to the reduction of CeO_2 as excessive copper addition would destroy Sb-Ce-Zr structures and lead to the formation of pure CeO_2 crystals. Furthermore, focusing on the changes of the reduction peak ascribed to Ce-O-Sb structure, it could be obviously found that the reduction peak was slowly weakened. The above results demonstrated that the pristine existed Sb-Ce-Zr interactions in SCZ sample were disrupted by the addition of Cu, which fitted well with the TEM and XPS results. Importantly, although the Sb-Ce-Zr interactions were interfered, the high strong reducibility of Cu still obviously enhanced the redox ability of the catalysts, which was responsible for the increased removal efficiency of methanol and NO_x at low temperature.

3.4 Effects of copper modification on the behaviors of various reactants

For the mixed pollutants, the overall removal efficiency is closely related to the reaction behaviors of various reactants (i.e., CH_3OH, NO_x, and NH_3). Therefore, various characterizations were conducted to analyze the changes of the adsorption of reactants on the catalyst surface after the Cu addition. Additionally, the two representative samples SCZ and $Cu_{0.05}$SCZ were selected for comparison. As shown in Figs. 6a and 6b, the Cu modification could significantly influence the formation of nitrogenous species on the catalyst. Specially, compared to the SCZ sample, the $Cu_{0.05}$SCZ sample desorbed more NO and NO_2 above 350 °C in the absence of methanol, indicating that more adsorbed nitrate species could participate in SCR reaction on the Cu-modified sample (Kang et al., 2019). The nitrogenous species on $Cu_{0.05}$SCZ sample were mainly desorbed in the form of NO_2 due to the improved strong oxidation capacity. With the co-adsorption of methanol, the desorbed concentration of NO and NO_2 would be significantly suppressed on both

samples, suggesting that methanol could greatly inhibit the adsorption of nitrate species on both catalysts surface. However, the residual desorption peak area of NO and NO_2 on $Cu_{0.05}$SCZ sample was still much higher than that of SCZ sample in the presence of methanol, indicating more nitrate species could be reserved to participate in the NH_3-SCR reaction. And it was beneficial to alleviate the decline of NO_x conversion in the presence of methanol. Similarly, the DRIFT spectra in Fig. 6c also demonstrated that the Cu modification could enhance redox capacity and then improve the adsorption of NO_x in the presence of methanol, as the peaks ascribed to nitrate species (1614, 1538, and 1246 cm^{-1}) emerged much more faster on $Cu_{0.05}$SCZ sample under the condition of methanol pre-adsorption (Wu et al., 2007; Zhu et al., 2021). And the results were further verified by NO oxidation experiment on fixed bed reactor. From Fig. 6d, it could be found that the presence of methanol would reduce the NO_2 yield of SCZ sample to about 70% at 250 °C or 350 °C, where the oxidation of NO to NO_2 on the Cu-modified sample was slightly affected by methanol.

As shown in Fig. 7, the adsorption and reaction of ammonia on the two samples in the presence of methanol was also conducted by NH_3-TPD, NH_3-IR and ammonia oxidation experiment. From Fig. 7a, the total peak area of NH_3 desorption on the fresh $Cu_{0.05}$SCZ sample was very close to that of the SCZ sample. However, when the samples were pre-treated by methanol, more NH_3 released from $Cu_{0.05}$SCZ sample at 300–400 °C. The extra part of NH_3 desorption could be ascribed to the decomposition of formamide species (Zhu et al., 2021), as a stronger sharp peak located at 1678 cm^{-1} could be detected on the $Cu_{0.05}$SCZ sample pretreated with methanol in Fig. 7b. Additionally, the results of NH_3 oxidation (see Figs. 7c and 7d) illustrated that the activation of NH_3 was improved to some extent after Cu modification, which was in accordance with previous enhanced redox ability results. Importantly, the existence of methanol possessed lesser inhibitory effect on $Cu_{0.05}$SCZ compared to SCZ sample, where the NH_3 conversion rate of the $Cu_{0.05}$SCZ sample was much higher than that of SCZ sample during the temperature range of 100–350 °C in the presence of methanol. Therefore, it could be concluded that Cu modification would make the NH_3 activation easier in the presence of methanol at low-medium temperatures and then promote simultaneous catalytic abatement performance of methanol and NO_x at low temperatures. Above 350 °C, compared with SCZ sample, the higher generated NO_x concentration in the tailed gas of $Cu_{0.05}$SCZ sample was ascribed to the over-oxidation of NH_3, and it was the reason of the decreased SCR activity at high temperatures (Wang et al., 2018; Wang et al., 2020b). Moreover, more NO_x generated in the presence of methanol were observed over both samples, which might be due to the suppressed NH_3-SCO reaction by methanol.

Additionally, the influence of the adsorbed methanol on the NH_3-SCR reaction via the E-R pathway had also been investigated by DRIFT spectra. From the variation trend

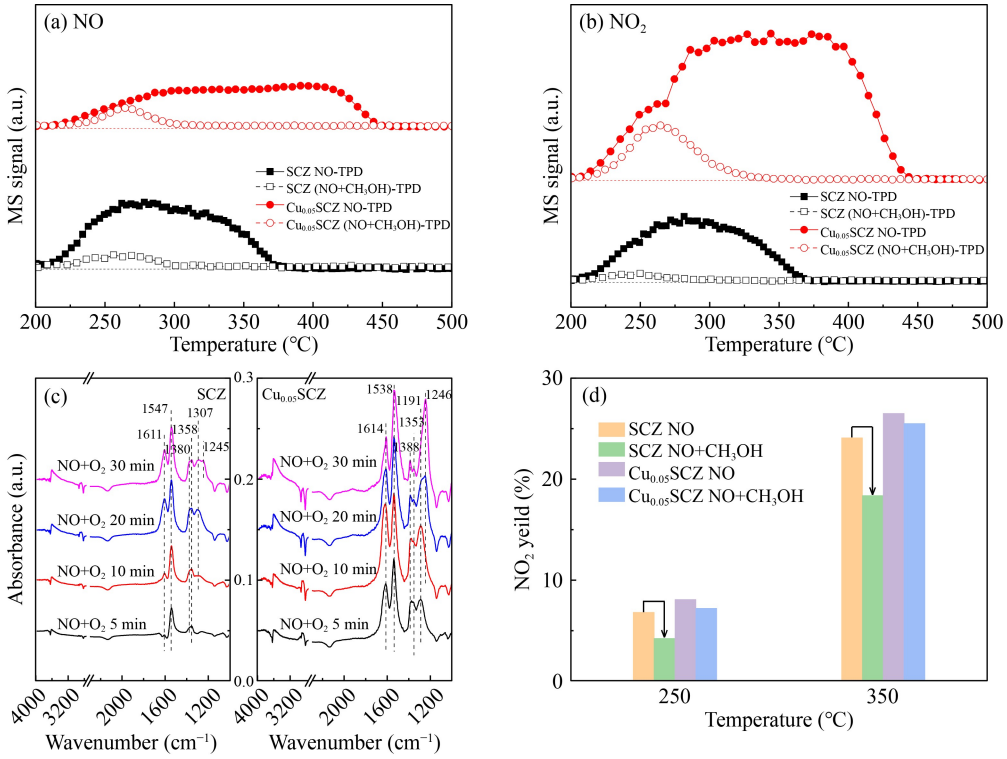

Fig. 6 The mass signal of NO-TPD experiment: (a) NO and (b) NO_2; (c) DRIFT spectra of NO + O_2 on catalysts pretreated with methanol; (d) Evolution of NO_2 during NO oxidation over SCZ and $Cu_{0.05}$SCZ samples.

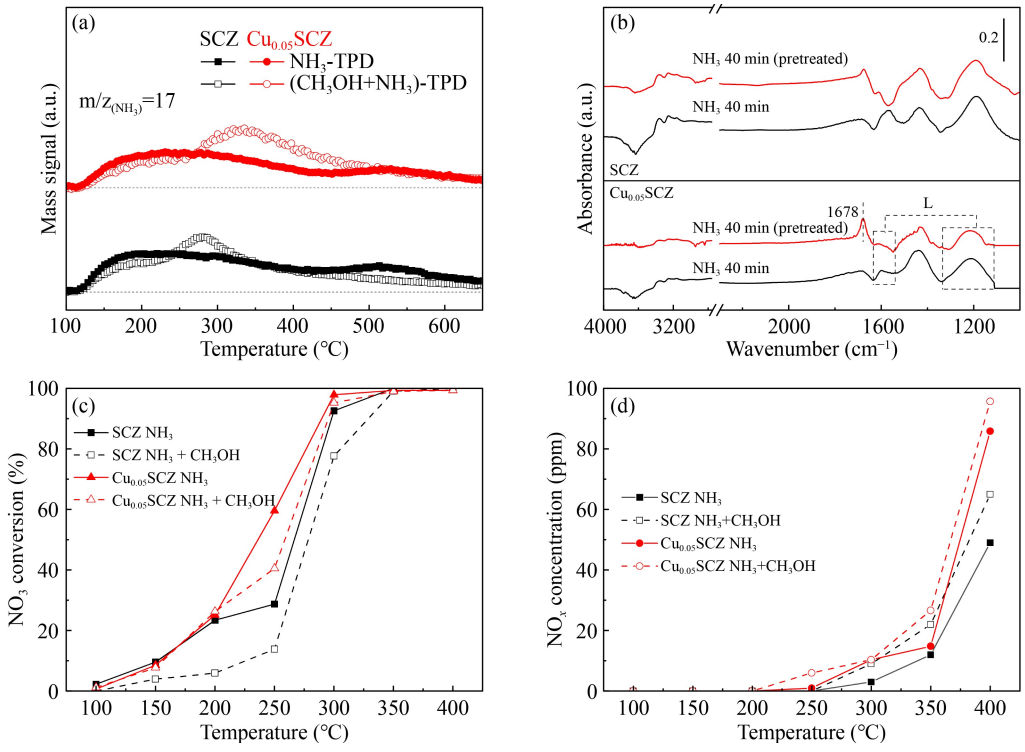

Fig. 7 The influence of methanol on (a) NH_3-TPD, (b) NH_3-IR and NH_3 oxidation results: (c) NH_3 conversion and (d) evolution of NO_x of SCZ and $Cu_{0.05}$SCZ samples.

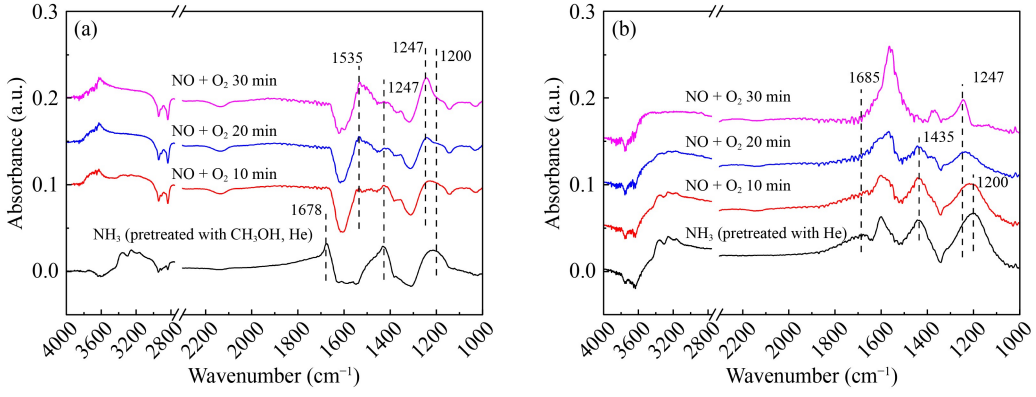

Fig. 8 DRIFT spectra of E-R reaction pathway on the $Cu_{0.05}$SCZ sample: (a) pretreated with methanol/He; (b) pretreated with He.

of the peak at 1200 cm^{-1} in Fig. 8, it could be observed that the reaction between NH_3 adsorbed at Lewis acid site and gaseous NO was slightly inhibited by the adsorbed methanol, since this peak did not totally vanish after 30 min NO + O_2 exposure. As a result, the NO_x conversion of copper modified catalyst in the presence of methanol still lower than that without methanol feed in. Meanwhile, the accumulation rate of nitrates (peaks located at 1535 and 1247 cm^{-1}) on the surface slowed down with the methanol pretreatment, indicating that the adsorbed methanol could inhibit the formation of nitrates, which was in consistent with the DRIFT results of NO + O_2 adsorption (see Fig. 6c). This phenomenon was similar to the case of SCZ catalyst reported previously (Zhu et al., 2021). Notably, it could be found that there were significant differences between two catalysts for the variation of the peak corresponding to the formamide species (~1678 cm^{-1}). The peak at 1678 cm^{-1} was rapidly disappeared after the exposure of NO + O_2, while that were relatively stable for pure SCZ sample (Zhu et al., 2021). Such facts could be due to two main reasons. First, after copper addition, the enhanced redox capacity led to a reduction in the formation of carbonaceous species derived from incomplete oxidation of methanol on the surface. It was further verified by TPO experiments on the used SCZ and $Cu_{0.05}$SCZ catalysts. As shown in Fig. S6, it could be found that one strong CO_2 emission peak located at about 250 °C released from the two samples, which should be ascribed to the physical adsorbed CO_2 or carbonate species. Particularly, there existed another CO_2 emission peak located at around 350 °C in SCZ sample, which was due to the oxidation of carbon-containing

substances. And the above results indicated that lesser carbon deposited on $Cu_{0.05}SCZ$ sample compared with SCZ sample, which was due to the faster mineralization rate of methanol after copper modification. In addition, the intensified negative bands at around 3000 cm^{-1} due to methoxy species (Zhu et al., 2021) over $Cu_{0.05}SCZ$ catalyst also confirmed its stronger mineralization capacity toward methanol. Secondly, the reaction rate between the formed formamide species with NO + O_2 was accelerated on $Cu_{0.05}SCZ$ catalyst compared to SCZ sample. Based on our previous work (Zhu et al., 2021), the adsorbed formamide species were inert to participate in SCR reaction, leading to the decreased reaction rate of SCZ catalyst. Thus, in conclusion, the speedup of the formamide species by the Cu modification was also one of the reasons for the improved deNO_x activity at low-medium temperatures in the presence of methanol.

4 Conclusions

The catalytic performance for the Sb-Ce-Zr mixed oxides in the simultaneous abatement of methanol and NO_x could be improved by appropriate Cu modification, and the mechanism was discussed in this work. The main conclusions were listed as follows:

(1) Cu modification could improve the total oxidation of methanol and alleviate the inhibition effect of methanol on the NH_3-SCR efficiency. However, excessive Cu addition would be harmful to the SCR activity at high temperatures due to the over-oxidation of ammonia. Among the catalysts investigated in this work, the optimal $Cu_{0.05}SCZ$ sample showed good stability and activity at 250 °C with a NO_x conversion of 96% and a CO_2 yield of 97%, increased by 8% and 11% compared to the SCZ sample, respectively.

(2) Due to the strong Cu-Ce interactions, the redox capacity of the Cu-modified catalyst was enhanced, which was the fundamental reason for the improvement of methanol total oxidation. However, excessive Cu addition would destroy the crystal structure of Sb-Ce-Zr, resulting in the decrease of specific surface area and acidity of the catalyst.

(3) Cu modification could mitigate the inhibitory effects of methanol on the adsorption and oxidation of NO/NH_3, and also accelerate the conversion of formamide species on the surface, thus achieving a better simultaneous catalytic abatement performance of methanol and NO_x at low temperature.

Acknowledgements The authors acknowledge for the financial support of Fundamental Research Funds for the Central Universities (No. 2021XZZX025), National Natural Science Foundation of China (No. 22076164) and Research Startup Program of Jiaxing University (No. CD70520027).

Electronic Supplementary Material Supplementary material is available in the online version of this article at https://doi.org/10.1007/s11783-022-1565-0 and is accessible for authorized users.

References

Ali S, Chen L, Yuan F, Li R, Zhang T, Bakhtiar S U H, Leng X, Niu X, Zhu Y (2017). Synergistic effect between copper and cerium on the performance of Cu_x-$Ce_{0.5-x}$-$Zr_{0.5}$ (x = 0.1–0.5) oxides catalysts for selective catalytic reduction of NO with ammonia. Applied Catalysis B: Environmental, 210: 223–234

Ambekar A, Maurya A K, Chowdhury A (2018). Droplet combustion studies of nitromethane and its blends. Experimental Thermal and Fluid Science, 93: 431–440

Chu B, Ma Q, Liu J, Ma J, Zhang P, Chen T, Feng Q, Wang C, Yang N, Ma H, Ma J, Russell A G, He H (2020). Air pollutant correlations in China: Secondary air pollutant responses to NO_x and SO_2 control. Environmental Science & Technology Letters, 7(10): 695–700

Gan L, Li K, Niu H, Peng Y, Chen J, Huang Y, Li J (2021). Simultaneous removal of NO_x and chlorobenzene on V_2O_5/TiO_2 granular catalyst: Kinetic study and performance prediction. Frontiers of Environmental Science & Engineering, 15(4): 70

Gan L, Shi W, Li K, Chen J, Peng Y, Li J (2018). Synergistic promotion effect between NO_x and chlorobenzene removal on MnO_x-CeO_2 catalyst. ACS Applied Materials & Interfaces, 10(36): 30426–30432

Gao S, Chen X, Wang H, Mo J, Wu Z, Liu Y, Weng X (2013). Ceria supported on sulfated zirconia as a superacid catalyst for selective catalytic reduction of NO with NH_3. Journal of Colloid and Interface Science, 394(Supplement C): 515–521

Graham G W, Weber W H, Peters C R, Usmen R (1991). Empirical method for determining CeO_2-particle size in catalysts by Raman spectroscopy. Journal of Catalysis, 130(1): 310–313

Hu Z, Liu X, Meng D, Guo Y, Guo Y, Lu G (2016). Effect of ceria crystal plane on the physicochemical and catalytic properties of Pd/ceria for CO and propane oxidation. ACS Catalysis, 6(4): 2265–2279

Huang X, Wang D, Yang Q, Peng Y, Li J (2021). Multi-pollutant control (MPC) of NO and chlorobenzene from industrial furnaces using a vanadia-based SCR catalyst. Applied Catalysis B: Environmental, 285: 119835

Kang L, Han L, He J, Li H, Yan T, Chen G, Zhang J, Shi L, Zhang D (2019). Improved NO_x reduction in the presence of SO_2 by using Fe_2O_3-promoted halloysite-supported CeO_2-WO_3 catalysts. Environmental Science & Technology, 53(2): 938–945

Li C, Li Q, Lu P, Cui H, Zeng G (2012). Characterization and performance of V_2O_5/CeO_2 for NH_3-SCR of NO at low temperatures. Frontiers of Environmental Science & Engineering, 6(2): 156–161

Li W, Liu H, Chen Y (2017). Promotion of transition metal oxides on the NH_3-SCR performance of ZrO_2-CeO_2 catalyst. Frontiers of Environmental Science & Engineering, 11(2): 6

Liang Q, Li J, He H, Liang W, Zhang T, Fan X (2017). Effects of SO_2 on the low temperature selective catalytic reduction of NO by NH_3 over CeO_2-V_2O_5-WO_3/TiO_2 catalysts. Frontiers of Environmental Science & Engineering, 11(4): 4

Long Y, Su Y, Xue Y, Wu Z, Weng X (2021). V_2O_5-WO_3/TiO_2 catalyst for efficient synergistic control of NO_x and chlorinated organics: Insights into the arsenic effect. Environmental Science & Technology, 55(13): 9317–9325

Lu J, Wang J, Zou Q, He D, Zhang L, Xu Z, He S, Luo Y (2019). Unravelling the nature of the active species as well as the doping effect over Cu/Ce-based catalyst for carbon monoxide preferential oxidation. ACS Catalysis, 9(3): 2177–2195

Qu W, Liu X, Chen J, Dong Y, Tang X, Chen Y (2020). Single-atom catalysts reveal the dinuclear characteristic of active sites in NO selective reduction with NH_3. Nature Communications, 11(1): 1532

Reddy B M, Bharali P, Saikia P, Khan A, Loridant S, Muhler M, Grünert W (2007). Hafnium doped ceria nanocomposite oxide as a novel redox additive for three-way catalysts. Journal of Physical Chemistry C, 111(5): 1878–1881

Sun P, Yu H, Liu T, Li Y, Wang Z, Xiao Y, Dong X (2021). Efficiently photothermal conversion in a MnO_x-based monolithic photothermo-catalyst for gaseous formaldehyde elimination. Chinese Chemical Letters

Taniguchi T, Watanebe T, Ichinohe S, Yoshimura M, Katsumata K-I, Okada K, Matsushita N (2010). Nanoscale heterogeneities in CeO_2-ZrO_2 nanocrystals highlighted by UV-resonant Raman spectroscopy. Nanoscale, 2(8): 1426–1428

Wang B, Wang M, Han L, Hou Y, Bao W, Zhang C, Feng G, Chang L, Huang Z, Wang J (2020a). Improved activity and SO_2 resistance by Sm-modulated redox of $MnCeSmTiO_x$ mesoporous amorphous oxides for Low-Temperature NH_3-SCR of NO. ACS Catalysis, 10(16): 9034–9045

Wang D, Chen Q, Zhang X, Gao C, Wang B, Huang X, Peng Y, Li J, Lu C, Crittenden J (2021a). Multipollutant control (MPC) of flue gas from stationary sources using SCR technology: A critical review. Environmental Science & Technology, 55(5): 2743–2766

Wang S, Fan C, Zhao Z, Liu Q, Xu G, Wu M, Chen J, Li J (2020b). A facile and controllable *in situ* sulfation strategy for CuCeZr catalyst for NH_3-SCR. Applied Catalysis A, General, 597: 117554

Wang X, Liu Y, Wu Z (2020c). Highly active $NbOPO_4$ supported Cu-Ce catalyst for NH_3-SCR reaction with superior sulfur resistance. Chemical Engineering Journal, 382: 122941

Wang X, Liu Y, Wu Z (2020d). The poisoning mechanisms of different zinc species on a ceria-based NH_3-SCR catalyst and the co-effects of zinc and gas-phase sulfur/chlorine species. Journal of Colloid and Interface Science, 566: 153–162

Wang X, Liu Y, Wu Z (2021b). Temperature-dependent influencing mechanism of carbon monoxide on the NH_3-SCR process over ceria-based catalysts. ACS ES&T Engineering, 1(7): 1131–1139

Wang X, Liu Y, Yao W, Wu Z (2019). Boosting the low-temperature activity and sulfur tolerance of $CeZr_2O_x$ catalysts by antimony addition for the selective catalytic reduction of NO with ammonia. Journal of Colloid and Interface Science, 546: 152–162

Wang X, Liu Y, Ying Q, Yao W, Wu Z (2018). The superior performance of Nb-modified Cu-Ce-Ti mixed oxides for the selective catalytic reduction of NO with NH_3 at low temperature. Applied Catalysis A, General, 562: 19−27

Wu Z, Jiang B, Liu Y, Wang H, Jin R (2007). DRIFT study of manganese/titania-based catalysts for low-temperature selective catalytic reduction of NO with NH_3. Environmental Science & Technology, 41(16): 5812–5817

Yao X, Chen L, Cao J, Chen Y, Tian M, Yang F, Sun J, Tang C, Dong L (2019). Enhancing the deNO_x performance of MnO_x/CeO_2-ZrO_2 nanorod catalyst for low-temperature NH_3-SCR by TiO_2 modification. Chemical Engineering Journal, 369: 46–56

Ye L, Lu P, Chen X, Fang P, Peng Y, Li J, Huang H (2020). The deactivation mechanism of toluene on MnO_x-CeO_2 SCR catalyst. Applied Catalysis B: Environmental, 277: 119257

Zeng Y, Haw K G, Wang Z, Wang Y, Zhang S, Hongmanorom P, Zhong Q, Kawi S (2021). Double redox process to synthesize CuO-CeO_2 catalysts with strong Cu-Ce interaction for efficient toluene oxidation. Journal of Hazardous Materials, 404: 124088

Zhai S, Su Y, Weng X, Li R, Wang H, Wu Z (2021). Synergistic elimination of NO_x and chlorinated organics over VO_x/TiO_2 catalysts: A combined experimental and DFT study for exploring vanadate domain effect. Environmental Science & Technology, 55(19): 12862–12870

Zhang X, Xuan Y, Wang B, Gao C, Niu S, Zhao G, Wang D, Li J, Lu C, Crittenden J C (2022). Precise regulation of acid pretreatment for red mud SCR catalyst: Targeting on optimizing the acidity and reducibility. Frontiers of Environmental Science & Engineering, 16(7): 88

Zhou G, Maitarad P, Wang P, Han L, Yan T, Li H, Zhang J, Shi L, Zhang D (2020). Alkali-resistant NO_x reduction over SCR catalysts via boosting NH_3 adsorption rates by *in situ* constructing the sacrificed sites. Environmental Science & Technology, 54(20): 13314–13321

Zhu Y, Zhou F, Wang X, Liu Y, Wu Z (2021). Reaction behaviors of NO_x and methanol simultaneous abatement over a ceria-based NH_3-SCR catalyst at low-medium temperatures. Journal of Physical Chemistry C, 125(27): 14666–14674